Quantum Chemical Modeling of Ethene Epoxidation with Hydrogen Peroxide: The Effect of Microsolvation with Water

Angelica Lundin,[†] **Itai Panas,*,**[‡] **and Elisabet Ahlberg**[†]

Department of Chemistry, Electrochemistry Göteborg University, S-412 96 Göteborg, Sweden, and Department of Chemistry and Biotechnology, Chalmers University of Technology, S-412 96 Göteborg, Sweden

Received: April 16, 2007; In Final Form: July 13, 2007

Quantum chemical calculations were performed to study the mechanism of ethene epoxidation with hydrogen peroxide. The calculations were carried out at the B3LYP/6-311+G(d,p) level of theory. The applicability of this functional to the problem at hand, including basis set effects, was validated by CCSD(T) and CASSCF based multireference MP2 calculations. A mechanism was determined where hydrogen peroxide becomes polarized in the transition state upon binding to the ethene molecule. The distant hydroxide fragment of the attached hydrogen peroxide molecule becomes partly negatively charged, while the other part of the molecule involves a proton and becomes partly positively charged. In the absence of water an activation energy of 139.7 kJ mol^{-1} was determined for the isolated H_2O_2 + C_2H_4 system. By microsolvating with water, the impact of a hydrogen-bonded network on the activation energy was addressed. A 43.7 kJ mol^{-1} lowering of the activation energy, ΔE_a, was observed when including up to 4 water molecules in the model. This effect results from the stabilization of the proton and hydroxide fragments in the transition state. The findings are discussed in the context of previous theoretical studies on similar systems. Effects of adding or removing a proton to mimic acidic and alkaline conditions are addressed and the limitations of the model in solvating the excess charge are discussed.

1. Introduction

Selective epoxidation of alkenes with clean oxidants is an important goal of catalysis research. A variety of epoxides are produced and used on a large scale and, therefore, clean production methods are important for minimizing the environmental impact of the chemical industry.[1] Commercially, direct oxidation of ethene with oxygen is made in the gas phase using silver as a catalyst. The process is thermodynamically favorable but the conversion is kinetically hindered. The mechanism is still under debate but an understanding of the reaction has advanced by combined experimental and theoretical efforts.[2,3] The mechanism involves adsorption of molecular oxygen on the silver surface, forming a highly reactive silver oxide on the surface in parallel with epoxide formation. Recently, two different oxygen phases were detected on silver by STM and their existence was followed up by DFT calculations.[4–6] Epoxidation was shown to take place through an oxametallacycle with the ring closure as the rate-limiting step.[2] By synthesizing stable oxametallacycles and comparing experimental and theoretical vibration spectra it was proposed that surface oxametallacycles are precursors in the silver-catalyzed epoxidation of ethene.[3] For ethene the selectivity observed experimentally is high approaching the theoretical 86%, assuming that six out of seven ethene molecules form ethylene oxide and one undergoes total combustion, and the yield is good. However, for alkenes with allylic hydrogens this method cannot be used but great hope is instead associated to the epoxidation in zeolite compartments. The latter are modified to include

hydrophilic surface groups, resulting from hydrolysis of Si(IV)–O–Ti(IV) bridges, and include molecular water, which provide absorption domains for hydrogen peroxide as well as sited for catalytic epoxidation. Trends in the energetics for the hydrolysis of M–O–M bridges are presented in refs 7 and 8, while the double nature of molecular water in water-rich and water-poor compartments was discussed in relation to gel formation in nanosized silicon dioxide and in particular to anomalous interactions between molecular water and a hydroxylated inner surface.[9] Also, several preparative routes to epoxides are known in organic chemistry. However, many of these routes give undesired byproducts and more selective and environmentally friendly preparation routes are sought.

The most straightforward method of producing epoxides is by the direct addition of an oxygen atom. This is administrated in various schemes which involve activation of molecular oxygen. In this context, hydrogen peroxide is a good choice since it is a cheap and environmentally friendly oxidant where the only byproduct is water. Epoxidations with hydrogen peroxide have recently been reviewed.[1] Strategies for electro-catalytical synthesis of hydrogen peroxide on quinones[10] and at CoOOH surfaces[11] have previously been addressed and in situ generation of hydrogen peroxide for epoxidation has been suggested.[12] However, for some applications the oxidative strength of hydrogen peroxide is understood not to suffice. Direct pathways exist where metal complexes are utilized as catalysts for the epoxidation of olefins with O_2.[13–19] These are complemented by strategies where the peroxide is formed by treatment of the complex catalyst with hydrogen peroxide to form surface peroxide groups, which subsequently oxidize the olefin to form the desired product.[2,20–23] This two-step mechanism will be referred to as the *indirect pathway*, as opposed

---
* Address correspondence to this author. Phone: +46-31-772-2860. Fax: +46 31 772 2853. E-mail: itai@chalmers.se.
† Electrochemistry Göteborg University.
‡ Chalmers University of Technology.

The Effect of Microsolvation with Water

J. Phys. Chem. A, Vol. 111, No. 37, 2007 **9081**

TABLE 1: Hydrogen Peroxide Assisted Ethene Epoxidation in the Gas Phase at Different Levels of Theory.

method/basis set	$\Delta E_a{}^a$/kJ mol^{-1}	$\Delta E_R{}^a$/kJ mol^{-1}
B3LYP/6-31G(d,p)	149.6	−192.8
B3LYP/6-31+G(d,p)	140.6	−198.4
B3LYP/6-311+G(d,p)	139.7	−198.8
B3LYP/6-311+G(3df,3pd)	146.9	−203.0
BLYP/6-31G(d,p)	96.2	−175.3
BLYP/6-311+G(d,p)	85.7	−181.1
BLYP/6-311+G(3df,3pd)	93.2	−185.3
BP86/6-31G(d,p)	94.1	−193.8
BP86/6-311+G(d,p)	81.4	−201.8
BP86/6-311+G(3df,3pd)	89.5	−205.7

^{a} Zero-point corrected energies at 0 K.

to the *direct pathway* where the H_2O_2 reacts with the olefin to form epoxide in a single step.[24,25]

In what follows, a detailed mechanistic investigation is undertaken to understand the gas-phase reaction and the effect of microsolvation with water in accord with the *direct pathway*. Emphasis is given to the effects of a local hydrogen-bonded network on the activation energy for epoxidation. This is modeled by including explicit water molecules into the H_2O_2 + C_2H_4 system. The structures thus resemble those investigated by others employing surface hydroxide groups and coordinated water.[20,21,23,24] Effects on the activation energy of proton addition and proton removal with respect to the nH_2O + H_2O_2 + C_2H_4 ($n = 0-5$) clusters are also investigated. The results are taken here to model possible catalytic properties of partly hydrated and hydroxylated inner surfaces of zeolites. However, in the present work a catalytic site is not involved while in a forthcoming paper the additional effect of a metal ion site will be presented.

2. Methodological Considerations and Computational Details

Different model theories have been employed in earlier studies on epoxidation reactions. Most relevant in this context are the studies of Wells et al.[23,25] using a BPW91/LANL2DZ description for the calculations on catalytic propylene epoxidation in the gas phase and Vayssilov and van Santen,[24] who employed a BPVWN/VDZP description. Quantum chemistry based on density functional theory (DFT) has been applied throughout this study as well. However, this choice of methodology is not an obvious one, since the epoxidation of ethene by hydrogen peroxide involves the breaking of three bonds and the formation of three new bonds. Since activation energies are sought, transition state structures and energies are computed and thus it may be asked to what extent Kohn Sham DFT is at all applicable at the transition states, where bond dissociations are expected to result in small HOMO−LUMO gaps, which in turn would cause the breakdown of the KS DFT approach.

As summarized in Table 1 three different functionals have been used: hybrid B3LYP,[26,27] GGA BP86,[28−30] and BLYP[27,28] combined with different sizes of Pople's basis sets.[31,32] The two GGA functionals give a different class of activation energies than the hybrid functional and the difference in activation energy ranges from 53.4 to 58.3 kJ mol^{-1} depending on the basis set. In what follows, the origin of this discrepancy is discussed and justification for B3LYP as the functional choice provided.

CCSD(T)[33] calculations were performed on the smallest relevant system to test the applicability of the Kohn Sham DFT approach for the transition states. A number of CCSD(T) calculations for a series of different basis sets were performed

to estimate limiting activation energies (see Table S1 in the Supporting Information). A lower bound of 198.7 kJ mol^{-1} is obtained at the CCSD level of theory. However, introduction of perturbative triple-excitations out of the reference wave function has a striking effect on the energetics, i.e., a 125.5 kJ mol^{-1} lower bound to the CCSD(T) activation energy is estimated. The effect of the triples is due to the strained electronic structure at the transition state, which has characteristics of both ionic and covalent nature. Formally, the importance of the triplets would render the applicability of DFT highly questionable. Yet, DFT is expected to at least describe the heterolytic dissociation channel well, which is also the one leading to the relevant products. Justification for applying DFT in what follows is partly that trends rather than absolute values will be addressed, and that the importance of the heterolytic channel for catalytic epoxidation of olefins will be emphasized (see the Discussion). Having said this, it is remarkable how the B3LYP is successful in estimating the CCSD(T) activation energy, given that the importance of the triple excitations reflects large contributions corresponding to static correlation. Indeed, it has been suggested that it is the balance between the effective and explicit exchange interactions in the B3LYP hybrid functional that, by accident, is responsible for the surprisingly good description of systems displaying static correlation but in principle should be inappropriate for DFT.[34,35] This agreement becomes even more impressive if it is taken into account that the triples are introduced perturbatively, and thus their effect on the activation energy may be somewhat exaggerated. This was tested by performing multireference MP2 calculations based on CASSCF(8,8) calculations (CASSCF MR MP2).[36] By employing the 6-311+G(d,p) basis set an activation energy of 133.0 kJ mol^{-1} was obtained. This result is consistent with the conclusions drawn based on the CCSD(T) results. While there are still uncertainties associated with the degree to which the B3LYP functional correctly predicts the activation energy for epoxidation, it is certainly the functional preferred for the system of choice.

A valence triple-ζ basis set, 6-311+G(d, p),[32] was employed in all the B3LYP DFT calculations. This choice is justified by the importance of having a sufficiently accurate description of the hydrogen bonds. A balanced description of the hydrogen-bonding network is crucial in the present study because it deals with the effects of microsolvation, which results from the introduction of explicit water molecules. The particular choice of basis set results from the investigation of the $H_3O_2{}^-$ system. Two qualities should be satisfied for the basis set of choice, the reproduction of the subtle symmetry breaking in $H_3O_2{}^-$, which is taken as a sensitive signature to be satisfied by the basis set of choice, and a correct description of hydrogen bond stability, Table 2. The anion should have C_1 symmetry where the central hydrogen atom makes a bond to one oxygen atom and a hydrogen bond to the other one as opposed to C_2 symmetry where the hydrogen is equally shared between the oxygen atoms. Diffuse functions of heavy atoms are crucial in order to get a good description of this hydrogen bond. Increasing the number of polarization functions or the quality of the basis set is not sufficient to describe the hydrogen bond properly. In addition, the angle $\phi(H_1-O_2-H_2)$ has a more water-like (water 104.8°) description when adding diffuse functions. Thus, the crucial effect of adding a diffuse function is emphasized. In spite of the fact that the 6-31+G(d,p) basis set appears to be the most cost-effective description, the extension of the present study to include transition metal chemistry justifies the triple-ζ basis set.

TABLE 2: Test of Computational Methods and Basis Sets for the $H_3O_2^-$ Anion[a]

$$H_{''}^{'}O_1 - H_1 \overset{\phi}{\overset{\frown}{O_2}} \overset{H_2}{\underset{}{}} \qquad H_{''}^{'}O_1 - H_1 - O_2 \overset{H_2}{\underset{}{}}$$

$$C_1 \qquad\qquad\qquad C_2$$

method/basis set	O_1-H_1[b]	H_1-O_2[b]	$\phi(H_1-O_2-H_2)$[c]	C_1	C_2
B3LYP/6-31G(d,p)	1.233	1.233	97.7		C_2
B3LYP/6-31G(2d,2p)	1.288	1.288	97.9		C_2
B3LYP/6-31+G(d,p)	1.311	1.153	103.7	C_1	
B3LYP/6-31+G(2d,2p)	1.339	1.135	102.9	C_1	
B3LYP/6-31++G(d,p)	1.320	1.146	103.6	C_1	
B3LYP/6-311G(d,p)	1.228	1.228	97.1		C_2
B3LYP/6-311G(2d,2p)	1.228	1.228	97.0		C_2
B3LYP/6-311+G(d,p)	1.356	1.121	102.8	C_1	
B3LYP/6-311+G(2d,2p)	1.330	1.138	103.2	C_1	
B3LYP/6-311+G(3df,3pd)	1.345	1.129	103.1	C_1	
CCSD/aug-cc-pVDZ[42]	1.471	1.063	101.5	C_1	

[a] For proper description of hydrogen bonding, the C_1 symmetry description is required. [b] Bond lengths are given in Å. [c] Angles are given in deg.

All calculations were performed employing the GAUSSIAN 03 program package.[37] Molecular structures were optimized and analytical Hessians were subsequently evaluated for all the optimized geometries. All transition states are characterized by one negative eigenvalue of the Hessian matrix.

3. Results

The purpose of this study is to shed light on the mechanism of olefin epoxidation with hydrogen peroxide in confined geometries, e.g., interior of zeolites. Taking the reference system to be the simplest possible, i.e., $C_2H_4 + H_2O_2$ in the gas phase, effects on the activation energy are sought upon adding up to four water molecules under neutral, acidic, and alkaline conditions. The water network is introduced to investigate how the barrier for epoxidation is affected by microsolvation. The structure of the network is constructed such that the influence on barrier height upon stabilizing the charged fragments is obtained. Essential for the investigation is to ensure that the number of hydrogen bonds is the same in the reactant structure as in the transition state structure. Having this in place, all systems have been subject to full geometry optimization.

In alkaline media the hydrogen peroxide will be deprotonated to form the peroxide anion and in acidic media the oxonium H_3O^+ cation will be present in the model. In neutral and alkaline media the microsolvated hydrogen peroxide complex interacts only weakly with ethene or ethylene oxide and therefore these substances and the hydrogen peroxide/water complexes have been optimized separately. In acidic media the proton is attracted to the C−C double bond, the epoxide ring, and hydrogen peroxide and therefore the reactant, product, and TS have all been optimized as complexes. All energies are corrected for the zero-point vibrations (given in kJ mol^{-1} at 0 K) and the bonding distances are given in angstroms. In the following, changes in the bond distances for $O_\alpha-H$ and $O_\alpha-O_\beta$ of hydrogen peroxide, $C_\alpha-C_\beta$ for ethene, and $O_\alpha-C_\alpha$ and the $O_\alpha-C_\alpha-C_\beta$ angle of the transition state are given as a function of the number of microsolvated water molecules. These are key parameters in the reaction sequence and will be used together with the energetics in the discussion of the reaction mechanism.

3.1. Ethene Epoxidation in Neutral Media (N). In Figure 1 the reactants (**R xN**), products (**P xN**) and transition states (**TS xN**) are given as a function of the number of microsolvating water molecules (x). All structures are geometrically optimized
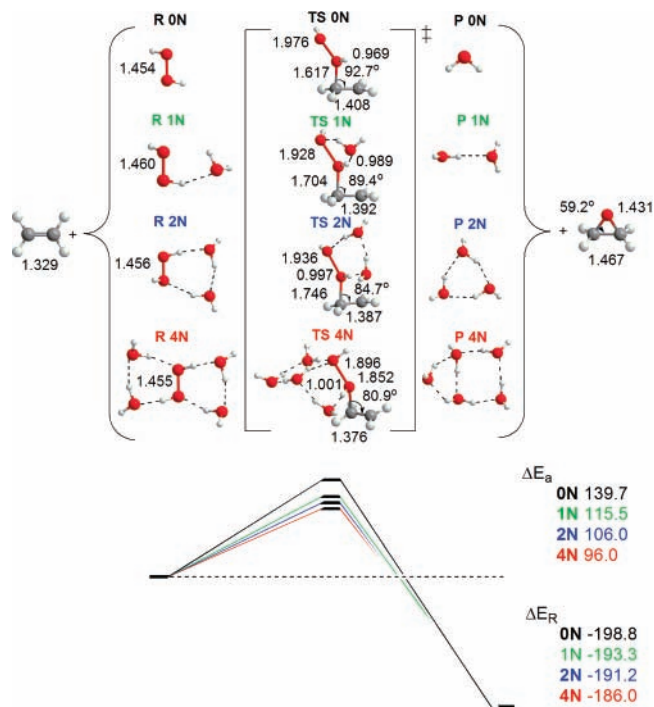

Figure 1. Hydrogen peroxide assisted ethene epoxidation with microsolvation with up to four water molecules. Bond distances are given in Å and energies at 0 K in kJ mol^{-1}. The activation and reaction energies, ΔE_a and ΔE_R, are given with respect to ethene and the microsolvated hydrogen peroxide.

and relevant bond distances are given in the figure. In the absence of water (**0N**) the hydrogen peroxide O−O bond is elongated in the transition state (**TS 0N**) from 1.454 Å to 1.976 Å as the bond is breaking up. The C−C bond is elongated from 1.329 Å in ethene to 1.408 Å in the transition state because of the double bond breaking. Negligible elongation of the $O_\alpha-H$ bond, 0.967 Å to 0.969 Å, is observed, while the $C_\alpha-O_\alpha$ distance is within bonding distance, 1.617 Å, as compared with the C−O bond in the epoxide product, 1.431 Å. The geometrical parameters of the $O_\beta-O_\alpha-C_\alpha-C_\beta$ backbone in the TS change upon microsolvating with water. The $O_\alpha-O_\beta$ bond distance decreases except for **TS 1N** 1.928 Å where the only water molecule keeps the $O_\alpha-O_\beta$ bond together with strong hydrogen bonds and is therefore shorter than in **TS 2N** 1.936 Å, The trends are in general decreasing the $O_\alpha-O_\beta$ bond distance, decreasing the $C_\alpha-C_\beta$ bond distance and, increasing the $C_\alpha-O_\alpha$ distance. These geometry changes indicate more reactant-like geometry of the TS upon increasing the number of water molecules. However, also the $O_\alpha-H$ bond increases and the $O_\alpha-C_\alpha-C_\beta$ angle decreases, thus indicating a product-like character of the TS.

The activation barrier decreases compared to that in the gas phase (139.7 kJ mol^{-1}) to 115.5 (**1N**), 106.0 (**2N**), and 96.0 (**4N**) kJ mol^{-1} when 1, 2, and 4 water molecules are added, respectively (Figure 1). The most pronounced effect is obtained with addition of one water molecule and most of the effect on the activation barrier is already observed after the addition of two water molecules. When four water molecules are present the $O_\beta-H$ entity has two hydrogen bonds indicative of a partly negative charge. Because of this charge and the presence of the $O_\alpha-O_\beta$, the $O_\beta-H$ entity will not coordinate a third water molecule. Given too that the local aspect of the $H_2O \leftarrow H-O_\alpha$ proton transfer is properly described, further addition of
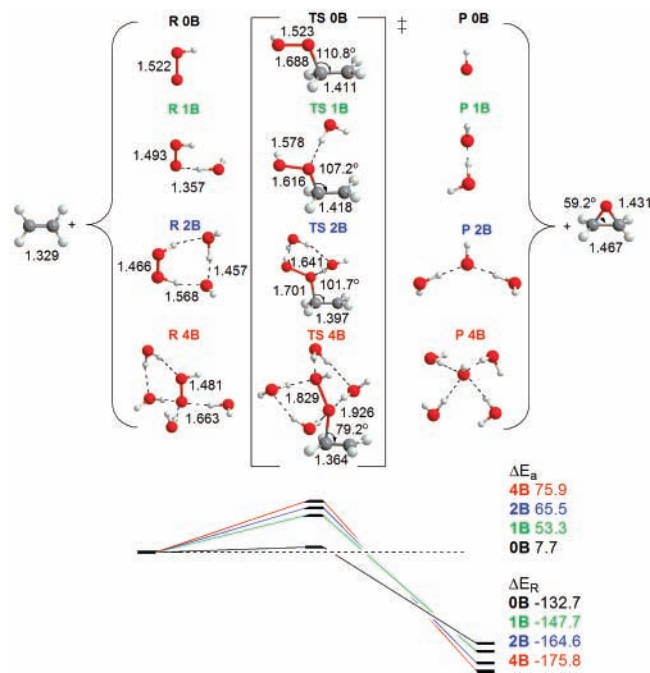
Figure 2. Ethene epoxidation with the hydrogen peroxide anion, HOO$^-$, microsolvated with up to four water molecules as a model for alkaline media. Bond distances are given in Å and energies at 0 K in kJ mol^{-1}. The activation and reaction energies, ΔE_a and ΔE_R, are given with respect to ethene and the microsolvated hydrogen peroxide anion.

microsolvating water molecules is not expected to significantly affect the activation barrier.

3.2. Ethene Epoxidation in Alkaline Media (B). The main difference compared to the neutral solution is the absence of proton transfer, i.e., the hydrogen peroxide will be deprotonated to an anion in alkaline solution. In Figure 2 the structures of the reactants (**R xB**), products (**P xB**), and transition states (**TS xB**) are given as a function of the number of microsolvating water molecules (x). The O$_\alpha$–O$_\beta$ bond in **TS 0B** is about the same as that for the hydroperoxy anion, 1.523 and 1.522 Å, respectively. The C$_\alpha$–C$_\beta$ bond is elongated from 1.329 Å in ethene to 1.411 Å in the transition state because of the double bond breaking. The O$_\alpha$–C$_\alpha$ distance is within bonding distance, 1.688 Å, as compared with the O–C bond in the epoxide product, 1.431 Å. In **TS 0B** the C$_\alpha$–O$_\alpha$ is shorter than in **TS 1B**, 1.616 and 1.688 Å, respectively. This is due to the stabilization of the negative charge in **TS 1B** by a hydrogen bond to water, as opposed to **TS 0B** where the negative charge is repelled from the C$_\alpha$ atom and hence making the bond longer. Also the C$_\alpha$–C$_\beta$ bond is longer in **TS 1B** than in **TS 0B** because of the stabilization of the negative charge by the water molecule. Otherwise, the general trend is that the C$_\alpha$–C$_\beta$ bond distance decreases and the C$_\alpha$–O$_\alpha$ distance increases. These geometry changes again indicate a more reactant-like geometry of the TS. However, the O$_\alpha$–O$_\beta$ bond distance increases and the O$_\alpha$–C$_\alpha$–C$_\beta$ angle decreases, indicating a product-like character at the TS.

Compared to the gas phase the activation barrier increases from 7.7 kJ mol^{-1} (**0B**) to 53.3 (**1B**), 65.5 (**2B**), and 75.9 (**4B**) kJ mol^{-1} when microsolvating with 1, 2, and 4 water molecules, respectively (see Figure 2). This is because the transition states are less stabilized by microsolvation than are reactants and products. This is why the activation energies increase upon increasing the number of water molecules. As in the neutral case when four water molecules are present, there will be two hydrogen bonds stabilizing the distant O$_\beta$ and in addition two
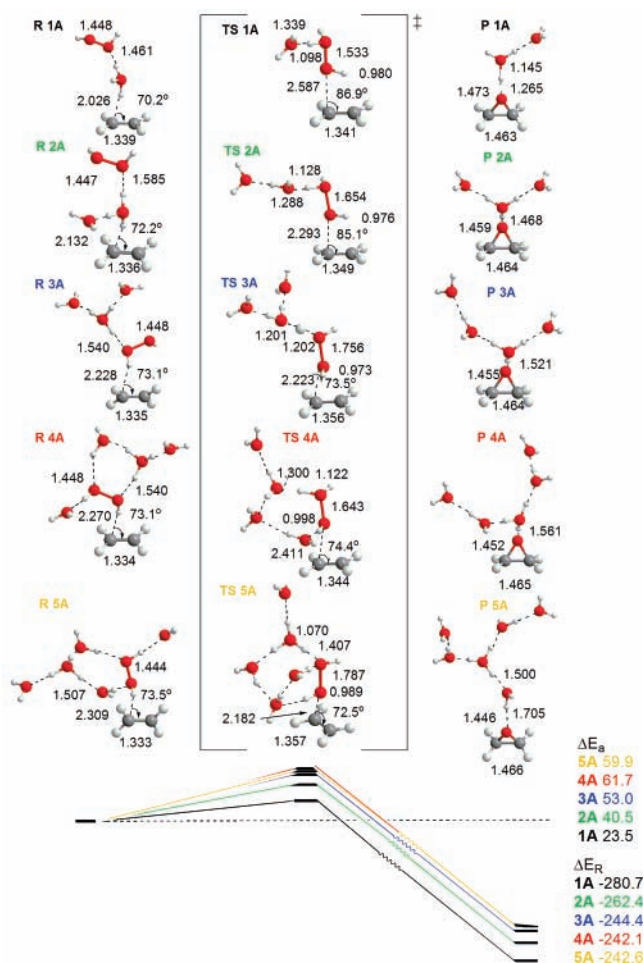

Figure 3. Ethene epoxidation with hydrogen peroxide in the presence of an oxonium cation, H$_3$O$^+$, microsolvated with up to four water molecules as a model for acidic media. Bond distances are given in Å and energies at 0 K in kJ mol^{-1}. The activation and reaction energies, ΔE_a and ΔE_R, are given with respect to the microsolvated complexes involving ethene and hydrogen peroxide.

hydrogen bonds stabilizing the proximal O$_\alpha$. Therefore, the oxygen atoms are fully coordinated with hydrogen bonds and further water will not influence the barrier significantly.

3.3. Ethene Epoxidation in Acidic Media (A). In acidic media the proton will interact with the double bond of ethene, the epoxide, and hydrogen peroxide and therefore the products, TS, and reactants are optimized as complexes (Figure 3). Several configurations have been considered for each complex. The H$_3$O$^+$ cation will interact stronger with water and hydrogen peroxide than with the double bond. Thus, in **R 1A** and **R 2A** the configuration with the cation hydrogen bonded to the double bond will be lowest in energy (Figure 3). However, when more water molecules are present as in **R 3A**–**R 5A** the configuration with hydrogen peroxide hydrogen bonded to the double bond is lower in energy. In acidic media the epoxide is partly protonated but when more water molecules are surrounding the cation, the hydrogen bond to the epoxide becomes weaker. In **P 1A**–**P 4A** the configuration with the cation hydrogen bonded to the epoxide is lowest in energy but in **P 5A** a water molecule is hydrogen bonded to the epoxide. In **TS 1A**–**TS 5A** the cation will be strongly hydrogen bonded to the distant O$_\beta$.

Compared to **R 1A** the O$_\alpha$–O$_\beta$ bond in **TS 1A** is elongated from 1.448 Å to 1.533 Å as this bond is breaking up but the C$_\alpha$–C$_\beta$ bond is not affected, 1.339 Å in **TS 1A** compared to 1.341 Å in **R 1A**. O$_\alpha$ interacts weakly with the C$_\alpha$–C$_\beta$ double bond as reflected in the 2.587 Å O$_\alpha$–C$_\alpha$ distance. The trends
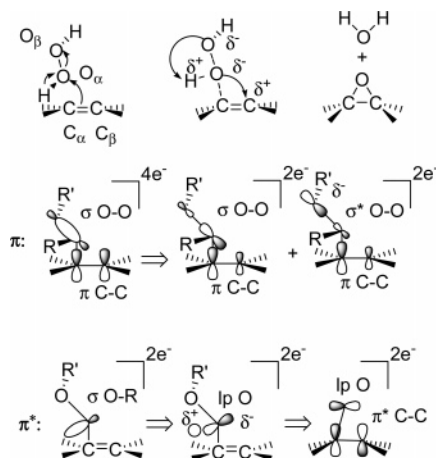
Figure 4. Mechanism of hydrogen peroxide assisted epoxidation of olefins. Two parts of the mechanism are depicted involving bonding π-orbitals and antibonding π*-orbitals of the olefin, respectively.

Figure 5. Electrostatic isopotentials (± 0.55 V) are displayed for **TS 0N** at the BLYP/DNP level of theory, i.e., double-ζ numerical basis set including polarization functions on each atom. Blue and yellow represent negative and positive isopotentials, respectively. The DMOL3 program package[43,44] as implemented in MATERIAL STUDIO[45] was used for these calculations.

are in general not as clear as in the neutral and alkaline case. This is due to the extra proton in the system that affects the hydrogen-bonded network strongly and thereby the O_β–O_α–C_α–C_β backbone. In general the O_α–O_β and C_α–C_β bond distances increase while the C_α–O_α bond distance and O_α–C_α–C_β angle decrease. One exception is **TS 4A** where the opposite trends hold compared with **TS 3A**. The reason for this is the presence of a water network bridge from O_α–H to the oxonium ion, which is not present in **TS 3A**. In **TS 5A** this bridge is present and in addition the distant O_β is stabilized by two hydrogen bonds instead of one as found in **TS 1A**–**TS 4A**. In **TS 1A**–**TS 3A** the O_α–H is not connected to the water network as in **TS 4A**–**TS 5A** and therefore the O_α–H distance decreases in **TS 1A**–**TS 3A** and increases in **TS 4A**–**TS 5A**.

The barrier in the presence of one oxonium ion (**1A**) is low, 23.5 kJ mol^{-1}, but it increases to 40.5 (**2A**), 53.0 (**3A**), 61.7 (**4A**), and 59.9 (**5A**) kJ mol^{-1} upon microsolvation by 1, 2, 3, and 4 additional water molecules, respectively (Figure 3). Further water molecules are not expected to affect the barrier significantly since the distant O_β–H unit is stabilized with two hydrogen bonds as in **TS 4N** and **TS 4B**.

4. Discussion

Oxidation of olefins by molecular oxygen must involve catalysts in order to activate the O_2 molecule and also to ensure epoxidation where thermodynamics would result in combustion.

Several catalysts for molecular oxygen activation have been developed, the purpose of which has been to produce active peroxide groups.[13,16,21,23,38−40] Indeed, the destabilization of the O_2 molecule upon peroxide formation is so great ($\sim$3 eV) that the actual process of epoxidation has been seen as a limiting property of an O_2 activating catalyst, rather than a separate problem with its own peculiarities. It is generally accepted that a peroxide species is required to break the double bond and enabling epoxide to be formed. Different ways of forming the active peroxide groups have been utilized like formation of peroxoacids, transition metal peroxo- and hydroperoxo complexes, and surface bound peroxide groups. Also in gas-phase reactions the role of hydrogen peroxide has been put forward in recent studies on the TiO$_2$/Au system.[41] Active peroxide groups are believed to form at the boundary between gold and titanium oxide by the reaction between H$_2$ and O$_2$. The selectivity for epoxide formation is high but the yield is low and the water formed in the reaction sequence is inhibiting the reaction by blocking the active sites.
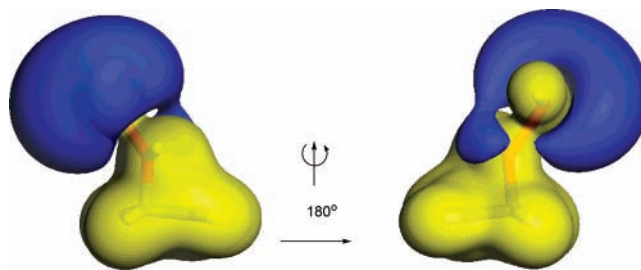
In this context, the present study seeks to determine general properties of an efficient catalyst for epoxidation of olefins by employing a preformed hydrogen peroxide as oxidant. Thus the major activation of the oxygen molecule has already been achieved, and what remains is the actual epoxidation reaction. Water molecules have been added to allow for microsolvation and to specifically investigate the role of a hydrogen-bonding network on the activation barrier. Thus, the epoxidation of ethene with hydrogen peroxide has been investigated both for gas-phase conditions and for reaction in the condensed phase. The role of hydrogen bonding on the stabilization of the hydrogen peroxide group has been discussed recently for alkene epoxidation with use of peroxycarboxylic acids.[24] One water molecule is formed in the catalyzed process and the proton transfer to hydrogen peroxide was shown to be rate limiting.[24] Further hydrogen bonding stabilizes the water molecule and facilitates the proton transfer to carboxylic oxygen.

The general results of the previous section can be summarized as follows: In the transition state, the C−C bond distance approaches that of free ethene as the microsolvation is improved, i.e., when more water molecules are added. The (O_α−C_α−C_β) angles in the transition state, which are 92.7° (neutral), 110.7° (alkaline), and 86.9° (acidic) for the bare reactions, are found in the range of 72−81° for the largest systems. The lowest converged activation energies are associated with the smallest (O_α−C_α−C_β) angles and the longest O−C distances except for acid conditions where the additional proton largely influences the hydrogen-bonded network. At the transition state, the distant OH group becomes negatively charged while the proximal group contains a proton. Stabilization of the charged fragments by the hydrogen-bonding network lowers the activation barrier.

The mechanism that emerges is depicted in Figure 4 and will be developed for the neutral case first, while effects of alkaline/acidic conditions will be discussed subsequently.

In the neutral case, the epoxidation reaction can be subdivided into a O−O dissociation part involving π-orbitals and an actual epoxidation part involving π*-orbitals. In case of the former, the electron pair in the σ bond is polarized toward the distant OH unit, thus producing a OH$^{\delta-}$ subunit. This polarization occurs in concert with the C=C π bond interacting with O_α, thus moving an electron pair into the $2p_\sigma(O_\alpha$−$O_\beta)$ from the back side. A shift of two electron pairs along the axis C_α→$O_\alpha O_\beta$H results and this part of the charge distribution can therefore be described in terms of the two subunits $[C_\alpha$→O_αH]$^{\delta+}$ and $[O_\beta$H]$^{\delta-}$. This can also be seen in Figure 5 where the isosurfaces for positive and negative electrostatic potentials for **TS 0N** are depicted for the BLYP functional, employed to approximate the B3LYP result. While properties such as energy are sensitive

The Effect of Microsolvation with Water

J. Phys. Chem. A, Vol. 111, No. 37, 2007 **9085**

to choice of functional, the electron density and thus the electrostatic potential are so to a much lesser extent, i.e., the B3LYP electron density can be approximated by that of BLYP. The actual epoxidation reaction occurs by the increasing interaction between one O_α lone-pair and the C=C π^* orbital. The accessibility of this lone-pair for bonding is enhanced by the polarization of the $[H^{\delta+}O_\alpha]$ subunit in conjunction with the increased overlap with the C=C π^* orbital. The reaction is completed when the $[H^{\delta+}O_\alpha]$ proton is allowed to recombine with the resulting $O_\beta H^-$ hydroxide ion. From the trends given in Figure 1 it can be observed that upon improving the microsolvation, the charged fragments in the transition state, $[H^{\delta+}O_\alpha]$ and $[O_\beta H]^{\delta-}$, become increasingly stabilized, thus bringing down the activation energy for the epoxidation reaction. The stabilization of the transition state implies preserving the reactant nature of both H_2O_2 and C_2H_4, which can be seen both in the $O_\alpha-C_\alpha-C_\beta$ angle which becomes increasingly more acute and the C=C bond distance which comes down from 1.408 Å to 1.376 Å upon microsolvation. It is gratifying to note how the proton donating property in the hydrogen bonds preferred by H_2O_2 in **R 1N**, **R 2N**, and **R 4N** is switched to the proton accepting property reflecting the partial anionic nature in the case of $[O_\beta H]^{\delta-}$, see particularly **TS 4N** in Figure 1.

Under alkaline conditions, the hydroperoxy anion HO_2^- is employed as oxidant. The same trend as that of the neutral system is observed in terms of more reactant-like structures as the number of molecules is increased in the microsolvated model (Figure 2). However, the activation energy is found to increase from 7.7 kJ mol^{-1} to 75.9 kJ mol^{-1}. This is because the reactant is stabilized to a significantly greater extent by microsolvation than the transition state. This can be understood by comparing **R 4B** to **TS 4B**, where water is seen to solvate the O^-_α by three molecules and the OH unit by one H_2O in the case of HOO^- (i.e., 3/1), whereas in the transition state the waters are distributed 2/2 (Figure 2). Because of steric hindrance, there is no space for additional water molecules in the vicinity of O^-_α in the transition state region. Even though microsolvation by four water molecules is not enough to converge the activation energies, the general features of the mechanism described above are recognized, comprising (1) a concerted move of two electron pairs along the axes $C_\alpha(\pi) \rightarrow O_\alpha$ and $O_\alpha \rightarrow O_\beta H$ and (2) overlap between an O_α 2p lone-pair with the C=C π^* orbital.

Under acidic conditions, the presence of the electron-withdrawing H_3O^+ subunit facilitates the stabilization of the $[O_\beta H]^{\delta-}$ fragment by the strong hydrogen bonds developed at the transition state. However, the very problem of solvating the excess proton keeps the TS reactant-like to a greater extent than in the alkaline and neutral systems, and yet, we observe the lowest activation energies for this system, i.e., ~60 kJ mol^{-1}. This is due to the effective stabilization of the $[O_\beta H]^{\delta-}$ subunit and the strong interaction between the $[H^{\delta+}O_\alpha]$ fragment with the neighboring water molecule. Thus, the mechanism outlined above is supported also for acidic conditions.

The efficiency of DFT in determining the geometries and energies of the transition states considered in the present study questions the validity of conventional understanding of catalytic epoxidation of olefins by H_2O_2, which has the O–O bond activation as its crucial element. Allowing for the energy splitting between the σ and σ^* states in the peroxide to decrease renders Kohn Sham DFT increasingly inapplicable. In contrast, decomposition by electron pairs displacements allows for the reaction to occur along a reaction path where the intermediate states are accessed by avoided crossings, such that the HOMO–LUMO gaps are sufficiently large everywhere(see Table 3). The

TABLE 3: HOMO−LUMO Gaps in Different Transition States.

TS	HOMO−LUMO gap^a/eV	TS	HOMO−LUMO gap^a/eV
TS 0N	2.93	**TS 2B**	3.91
TS 1N	3.43	**TS 4B**	4.98
TS 2N	3.70	**TS 1A**	4.28
TS 4N	4.12	**TS 2A**	4.29
TS 0B	3.55	**TS 3A**	4.40
TS 1B	3.68	**TS 4A**	4.52
		TS 5A	4.48

^{a} Calculated at the B3LYP/6-311+G(d,p) level of theory.

validity of the latter interpretation was tested by comparing the activation energy for the reaction **R 0N−TS 0N−P 0N** as obtained with B3LYP to those of CCSD(T) and CASSCF based MR MP2/6-311+G(d,p) (see Table S1, Supporting Information).

4.1. Solvation Effects in the Direct Epoxidation Reaction. It now becomes interesting to compare absolute activation energies as well as trends in ΔE_a for the epoxidation reaction to previous theoretical studies in the literature. Wells et al.[23] report 82.7 kJ mol^{-1} for the bare gas-phase reaction. This number is similar to the numbers obtained by other GGA functionals such as BLYP and BP86 when employing similar basis set qualities, whereas an activation energy of 139.7 kJ mol^{-1} is computed with B3LYP/6-311+G(d,p) (Table 1). The latter is supported by CCSD(T) ($E_a > 125.5$ kJ mol^{-1}) and CASSCF(8,8) MR MP2 (133.0 kJ mol^{-1}) results. Furthermore, Vayssilov and van Santen[24] give a 83 kJ mol^{-1} activation energy for ethene epoxidation by the *direct pathway* at a Ti(IV) site, i.e., without the formation of a hydroperoxy intermediate. This number was approximately reproduced by Wells et al. (75.1 kJ mol^{-1})[23] for propene epoxidation in a zeolite model catalyst. However, the similarity is due to the fact that in both cases the gas-phase reaction is probed, i.e., also in the presence of a catalytic site. The present study demonstrates that molecular water or hydroxide groups at the catalytic site should be able to reduce the gas-phase barrier by some 45 kJ mol^{-1}, which is significantly greater than the 7.6 kJ mol^{-1} (82.7−75.1 kJ mol^{-1}) shift reported in ref 23.

4.2. Destabilization of Reactants versus Stabilization of Transition State. A most striking result of the present study is how the introduction of a flexible hydrogen-bonding network is capable of lowering ΔE_a for the gas-phase system by some 45 kJ mol^{-1} owing to the stabilization of the transition state. Focus on transition state properties is opposite to efforts to activate the O−O bond by metal complex catalysts,[13,15,17−19] where differences in ΔE_a of up to 26 kJ mol^{-1} were obtained depending on the choice of activated peroxy complex. The latter was found to correlate with the stabilities of σ^* in the peroxy subunits. In this context, the purpose of the present study is to shift the attention somewhat from the activation of O_2 to the stabilization of the transition state. Indeed, support is presented here for an understanding where the efficiency of a catalyst for hydrogen peroxide assisted epoxidation has the stability of the transition state as the key element. In the transition state the stabilization of the $[O_\beta H]^{\delta-}$ leaving group is emphasized.

5. Conclusions

A new mechanism for hydrogen peroxide assisted epoxidation has been formulated, where the stabilization of the transitions state is emphasized. In the transition state, hydrogen peroxide is polarized to form a distant negatively charged hydroxide fragment and a proximal positively charged fragment due to proton formation. The reaction steps are discussed in terms of

displacements of electron pairs. This is as opposed to homolytic dissociation of electron pairs, for which the Kohn−Sham DFT approach is invalid. In this study the applicability of the B3LYP/6-311+G(d,p) description was justified by comparing to CCSD-(T) and CASSCF based multireference MP2 results.

Microsolvation with water leads to stabilization of the transition state and to a lowering of the activation energy, and a decrease of 43.7 kJ mol^{-1} is obtained. Hence, it was demonstrated how the hydrogen-bonding network acts as a catalyst for the epoxidation reaction by stabilizing the transition state.

Supporting Information Available: Activation energies of reaction **0N** with CCSD(T) and CASSCF MR MP2 comprising different basis sets are summarized in Table S1. This material is available free of charge via the Internet at http://pubs.acs.org.

References and Notes

(1) van Vliet, M. Selective Epoxidation with Hydrogen Peroxide, Delft University of Technology, 2001.

(2) Bareau, M. A. *Top. Catal.* **2003**, *22*, 3.

(3) Bocquet, M.-L.; Michaelides, A.; Offreda, D.; Sautet, P.; Alavi, A.; King, D. A. *J. Am. Chem. Soc.* **2003**, *125*, 5620.

(4) Bocquet, M.-L.; Sautet, P.; Cerda, J.; Carlisle, C. I.; Webb, M. J.; King, D. A. *J. Am. Chem. Soc.* **2003**, *125*, 3119.

(5) Carlisle, C. I.; King, D. A.; Bocquet, M.-L.; Cerda, J.; Sautet, P. *Phys. Rev. Lett.* **2000**, *84*, 3899.

(6) Michaelides, A.; Bocquet, M.-L.; Sautet, P.; Alavi, A.; King, D. A. *Chem. Phys. Lett.* **2003**, *367*, 344.

(7) Johnson, J. R. T.; Panas, I. *Chem. Phys. Lett.* **2001**, *348*, 433.

(8) Johnson, J. R. T.; Panas, I. *Inorg. Chem.* **2000**, *39*, 3192.

(9) Bjoernstroem, J.; Martinelli, A.; Johnson, J. R. T.; Matic, A.; Panas, I. *Chem. Phys. Lett.* **2003**, *380*, 165.

(10) Johnsson Wass, J. T. R.; Ahlberg, E.; Panas, I.; Schiffrin, D. J. *Phys. Chem. Chem. Phys.* **2006**, *8*, 4189.

(11) Johnsson Wass, J. T. R.; Panas, I.; Ásbjörnsson, J.; Ahlberg, E. *J. Electroanal. Chem.* **2007**, *599*, 295.

(12) Zimmer, A.; Mönter, D.; Reschetilowski, W. *J. Appl. Electrochem.* **2003**, *33*, 933.

(13) Deubel, D. V.; Frenking, G.; Gisdakis, P.; Herrmann, W. A.; Rösch, N.; Sundermeyer, J. *Acc. Chem. Res.* **2004**, *37*, 645.

(14) Gisdakis, P.; Antonczak, S.; Kostlmeier, S.; Herrmann, W. A.; Rosch, N. *Angew. Chem., Int. Ed.* **1998**, *37*, 2211.

(15) Gisdakis, P.; Rösch, N. *J. Phys. Org. Chem.* **2001**, *14*, 328.

(16) Gisdakis, P.; Yudanov, I. V.; Roesch, N. *Inorg. Chem.* **2001**, *40*, 3755.

(17) Rösch, N.; Di Valentin, C.; Yudanov, I. V. *Catal. Met. Complexes* **2002**, *25*, 289.

(18) Rösch, N.; Gisdakis, P.; Yudanov, I. V.; Di Valentin, C. *Peroxide Chem.* **2000**, 601.

(19) Yudanov, I. V.; Gisdakis, P.; Di Valentin, C.; Rosch, N. *Eur. J. Inorg. Chem.* **1999**, 2135.

(20) Sever, R. R.; Root, T. W. *J. Phys. Chem. B* **2003**, *107*, 4090.

(21) Sever, R. R.; Root, T. W. *J. Phys. Chem. B* **2003**, *107*, 4080.

(22) Sinclair, P. E.; Catlow, R. A. *J. Phys. Chem. B* **1999**, *103*, 1084.

(23) Wells, D. H.; Joshi, A. M.; Delgass, W. N.; Thomson, K. T. *J. Phys. Chem. B* **2006**, *110*, 14627.

(24) Vayssilov, G. N.; van Santen, R. A. *J. Catal.* **1998**, *175*, 170.

(25) Wells, D. H.; Delgass, W. N.; Thomson, K. T. *J. Am. Chem. Soc.* **2004**, *126*, 2956.

(26) Becke, A. D. *J. Chem. Phys.* **1993**, *98*, 5648.

(27) Lee, C.; Yang, W.; Parr, R. G. *Phys. Rev. B* **1988**, *37*, 785.

(28) Becke, A. D. *Phys. Rev. A* **1988**, *38*, 3098.

(29) Perdew, J. P. *Phys. Rev. B* **1986**, *33*, 8822.

(30) Perdew, J. P. *Phys. Rev. B* **1986**, *34*, 7406.

(31) Hehre, W. J.; Ditchfield, R.; Pople, J. A. *J. Chem. Phys.* **1972**, *56*, 2257.

(32) Krishnan, R.; Binkley, J. S.; Seeger, R.; Pople, J. A. *J. Chem. Phys.* **1980**, *72*, 650.

(33) Pople, J. A.; Head-Gordon, M.; Raghavachari, K. *J. Chem. Phys.* **1987**, *87*, 5968.

(34) Polo, V.; Grafenstein, J.; Kraka, E.; Cremer, D. *Chem. Phys. Lett.* **2002**, *352*, 469.

(35) Polo, V.; Kraka, E.; Cremer, D. *Mol. Phys* **2002**, *100*, 1771.

(36) McDouall, J. J. W.; Peasley, K.; Robb, M. A. *Chem. Phys. Lett.* **1988**, *148*, 183.

(37) Frisch, M. J.; Trucks, G. W.; Schlegel, H. B.; Scuseria, G. E.; Robb, M. A.; Cheeseman, J. R.; Montgomery, J. A., Jr.; Vreven, T.; Kudin, K. N.; Burant, J. C.; Millam, J. M.; Iyengar, S. S.; Tomasi, J.; Barone, V.; Mennucci, B.; Cossi, M.; Scalmani, G.; Rega, N.; Petersson, G. A.; Nakatsuji, H.; Hada, M.; Ehara, M.; Toyota, K.; Fukuda, R.; Hasegawa, J.; Ishida, M.; Nakajima, T.; Honda, Y.; Kitao, O.; Nakai, H.; Klene, M.; Li, X.; Knox, J. E.; Hratchian, H. P.; Cross, J. B.; Bakken, V.; Adamo, C.; Jaramillo, J.; Gomperts, R.; Stratmann, R. E.; Yazyev, O.; Austin, A. J.; Cammi, R.; Pomelli, C.; Ochterski, J. W.; Ayala, P. Y.; Morokuma, K.; Voth, G. A.; Salvador, P.; Dannenberg, J. J.; Zakrzewski, V. G.; Dapprich, S.; Daniels, A. D.; Strain, M. C.; Farkas, O.; Malick, D. K.; Rabuck, A. D.; Raghavachari, K.; Foresman, J. B.; Ortiz, J. V.; Cui, Q.; Baboul, A. G.; Clifford, S.; Cioslowski, J.; Stefanov, B. B.; Liu, G.; Liashenko, A.; Piskorz, P.; Komaromi, I.; Martin, R. L.; Fox, D. J.; Keith, T.; Al-Laham, M. A.; Peng, C. Y.; Nanayakkara, A.; Challacombe, M.; Gill, P. M. W.; Johnson, B.; Chen, W.; Wong, M. W.; Gonzalez, C.; Pople, J. A. *Gaussian 03*, Revision B.05; Gaussian, Inc.: Pittsburgh PA, 2003.

(38) Alder, R. W.; Davis, A. P. *J. Mol. Model* **2006**, *12*, 649.

(39) Di, Valentin, C.; Gisdakis, P.; Yudanov, I. V.; Roesch, N. *J. Org. Chem.* **2000**, *65*, 2996.

(40) Munakata, H.; Oumi, Y.; Miyamoto, A. *J. Phys. Chem. B* **2001**, *105*, 3493.

(41) Hayashi, T.; Tanaka, K.; Haruta, M. *J. Catal.* **1998**, *178*, 566.

(42) Woon, D. E.; Dunning, T. H., Jr. *J. Chem. Phys.* **1993**, *98*, 1358.

(43) Delley, B. *J. Chem. Phys.* **1990**, *92*, 508.

(44) Delley, B. *J. Chem. Phys.* **2000**, *113*, 7756.

(45) *MATERIAL STUDIO*; Accelrys inc., 2005.